



HAL
open science

Experimental study of the kinetics of degradation of n-dodecane under thermo-oxidative stress at low temperature and mechanism inferred

Soraya Aminane, Mickaël Sicard, Yanis Melliti, Frédéric Ser, Lorette Sicard

► To cite this version:

Soraya Aminane, Mickaël Sicard, Yanis Melliti, Frédéric Ser, Lorette Sicard. Experimental study of the kinetics of degradation of n-dodecane under thermo-oxidative stress at low temperature and mechanism inferred. *Fuel*, 2022, 307, pp.121669. 10.1016/j.fuel.2021.121669 . hal-03448533

HAL Id: hal-03448533

<https://hal.science/hal-03448533>

Submitted on 29 Nov 2021

HAL is a multi-disciplinary open access archive for the deposit and dissemination of scientific research documents, whether they are published or not. The documents may come from teaching and research institutions in France or abroad, or from public or private research centers.

L'archive ouverte pluridisciplinaire **HAL**, est destinée au dépôt et à la diffusion de documents scientifiques de niveau recherche, publiés ou non, émanant des établissements d'enseignement et de recherche français ou étrangers, des laboratoires publics ou privés.

Experimental study of the kinetics of degradation of *n*-dodecane under thermo-oxidative stress at low temperature and mechanism inferred

Soraya Aminane^a, *Mickaël Sicard*^{*a}, *Yanis Melliti*^a, *Frédéric Ser*^a, *Lorette Sicard*^b

a: DMPE, ONERA, Université Paris Saclay, F-91123 Palaiseau – France

b: Université de Paris, ITODYS, CNRS, F-75006 Paris, France

*E-mail: mickael.sicard@onera.fr

KEYWORDS: autoxidation, alkane, PetroOxy, kinetics

ABSTRACT

Autoxidation of jet fuels is a complex phenomenon which occurs below 250 °C. Caused by naturally dissolved oxygen, the reactions lead to the formation of different oxidation products by a mechanism of degradation which is not yet completely understood. *n*-dodecane, a linear alkane molecule, has been chosen as a model for jet fuel. The influence of temperature and progress of reactions have been studied using the PetroOXY device, focusing on the beginning of the autoxidation. For the first time, the oxidation products formed in the gas and liquid phases were precisely identified by spectroscopic and chromatographic characterization techniques but also

quantified by chemical methods. It was possible to establish the mechanisms involved in the different steps using data from the literature, to propose a new one based on combustion mechanisms and to calculate the kinetic constants of the reactions.

1. INTRODUCTION

Jet fuel, used for the propulsion of aircrafts, has a secondary less known function: it also serves as a cooling fluid; hence its temperature can outreach 200 °C. The thermal stress induced leads to its degradation and can entail the formation of solid deposition in the fuel system and multipoint injectors. This is a major issue in aeronautics as the deposition induces a loss of thermal transfer efficiency and can cause fouling in the injectors. To address this issue, it is of major importance to understand the mechanisms of degradation of jet fuel and to subsequently improve its thermal stability.

Thermal stability refers to the tendency of fuels to be degraded and to form soluble or insoluble oxidation products depending on the temperature range [1]. It includes autoxidation and thermal decomposition. The first results from the complex interactions between dioxygen, hydrocarbons and molecules with heteroatoms [2,3]. These reactions occur typically in the 140 to 250 °C temperature range. It is noteworthy that oxidation reactions have also been observed under storage stability conditions (temperatures \leq 140 °C) [4,5]. When the temperature reaches *ca.* 400 °C, thermal decomposition of the fuel starts to proceed more by pyrolysis. These temperature ranges alternate in aircraft engines during on-off operations.

Many experimental researches have been conducted to better understand the thermal stability of jet fuels [1-11]. They have highlighted the major role of dissolved oxygen in kerosene (*ca.* 70 ppm) in the degradation of hydrocarbon molecules and in the formation of insoluble compounds

[3,12-15,17]. Moreover, there is a significant contribution/role of heteroatomic species with respect to autoxidation and thermal decomposition reactions. It has been demonstrated in the literature that heteroatomic compounds have significantly more favorable activation energies, E_a , and readily participate in these oxidation reactions [20,25]. This is the reason why jet fuel may propagate under a slightly different pathway (or certainly different kinetic rates) compared to pure hydrocarbons.

Other studies have focused on the influence of physical factors on the degradation mechanisms, such as temperature [27,28], pressure [29,30], test duration, flow rate [31,32] and nature of the walls of the reactor [7,33,34]. These researches have made it possible to identify and quantify the insoluble products formed [3,8,10,35,36]. For example, Pei *et al.* [11] have proposed that the formation of deposits is a two steps mechanism with first, the formation, in the liquid phase, of precursor species which then migrates to the walls of the system, resulting in the progressive deposition of the particles.

Though the origin of insoluble products has been identified, the description of the autoxidation mechanisms remains rough and needs to be deepened. For this purpose, experimental devices allowing to simulate the thermal and flow conditions encountered in operational conditions have been developed. These tests are distinguished in two categories: dynamic and static tests. The first ones require a huge quantity of fuel, residence times are of a few seconds and the tests last for several hours [54]. Conversely, static tests require a low quantity of fuel and the test duration varies from 2 to 20 h for a temperature range from 140 to 250 °C [56-58,60,61,64,66,68].

Among the static tests, the PetroOXY device is typically used to study the tendency towards oxidation of petrol products and oils when Rapid Small Scale Oxidation Test (RSSOT) are required. Among the advantages are the low volume of samples and a good repeatability [75,78].

Using the PetroOXY to study the degradation of *n*-dodecane at 150 °C and 700 kPa, Sicard *et al.* [81] have evidenced the evolution of the degradation products with the conversion ($\Delta P/P = 10$ to 80 %). Chatelain *et al.* [82] also used this device to experimentally study the influence of the chain length and mixing of *n*-C₈-C₁₂ alkanes.

Since the 50s, many works have focused on establishing the mechanism of degradation. It implies the formation of radicals, which generates hydroperoxides, leading to the formation of alcohols, ketones, aldehydes and acids [37,39,53,55].

Garcia *et al.* [42] integrated kinetic aspects to propose the first simplified kinetic equations. It has been completed in 1994 by Heneghan [47] who proposed a simplified four-step mechanism, inspired from Zabarnick's works involving the formation of the first alkyl radicals R• during the initiation step and of RO₂H hydroperoxides during propagation. Several authors have used these equations to propose an autoxidation mechanism including all the species naturally present in kerosene [3,9,10,35,44-50].

Although the autoxidation of alkanes has been extensively studied experimentally, the works have mainly focused on the impact of dissolved oxygen on the formation of hydroperoxydes and deposits. The oxidation products have been identified but an accurate quantification in the gas and liquid phases, especially at the beginning of the reaction to understand the first steps, is still lacking. Moreover, no study has been able to clearly explain all the mechanisms involved in the degradation of hydrocarbons.

Regarding the kinetic aspect, although this last one has been exploited several times in the literature through the formalism of the Arrhenius law, we find few studies allowing to define explicitly the kinetic constants of degradation, allowing to predict the autoxidation reactions which are at the origin of the formation of precursors of deposits.

The objectives of this work are to study experimentally the autoxidation of a long chain linear alkane under thermal oxidative stress, to deepen the comprehension of the phenomenon, to confront the results to the existing kinetic models and to provide input to improve them. The implementation of a robust experimental protocol ensuring the repeatability of the tests as well as the identification and the quantification of the evolution of the reagents and the formation of the oxidation products was set up through various techniques of characterizations and chemical analysis.

n-Dodecane was chosen as a model for the fuel as (i) alkanes represent 40 % of the constituting molecules of jet fuel, and (ii) it has a high boiling point, 216.3 °C. The influence of different parameters (pressure drop and temperature) on the products obtained during its oxidation in a PetroOXY device has been studied and quantitative analysis of both the liquid and gas phases has been carried out. In a first step, the tests were carried out at fixed temperature (160 °C) and initial pressure of dioxygen (700 kPa) and stopped after different pressure drops ($\Delta P/P_{\max} = 2, 4, 6, 8$ and 10 %) to monitor the evolution of the oxidation products as a function of reaction time. In a second one, $\Delta P/P_{\max}$ was fixed at 10 % and the tests were made at three different temperatures (140, 150 and 160 °C) and an initial pressure of 700 kPa to understand the influence of these parameters on the stability of *n*-dodecane and determine the kinetics of degradation.

2. EXPERIMENTAL SECTION

2.1 PetroOXY device

The PetroOXY device (Anton Paar) was used to study the stability towards oxidation of the fuels [84]. 5 mL of *n*-dodecane (purity > 99 %, Alfa Aesar) is poured into a glass crucible. In order to assure that O₂ is the only dissolved gas, the fuel is degassed 2 minutes in an ultrasonic bath. The crucible is then introduced into a chamber hermetically closed. The initial static pressure of oxygen

is 700 kPa and the initial temperature is 160 °C. These physical features are continuously measured during the experiment. The test is stopped when a 10 % pressure decrease, relative to the maximum pressure measured, is reached. The induction period (IP) is defined as the duration between the maximum pressure and a 10 % fall.

All the samples are tested 4 times to verify the repeatability and to have enough oxidized liquid to characterize. After the test, the gas and liquid phases are recovered after cooling down the device to 25 °C.

2.2 Gasification rate and conversion rates of dioxygen and n-dodecane

At the end of the test, the liquid phase is collected and weighted. The gasification rate is calculated according to the formula:

$$\text{Gasification rate (\%)} = \frac{(m_i - m_f - m_s)}{m_i} \times 100$$

where m_i and m_f are the initial and final mass of *n*-dodecane, respectively, and m_s the mass of solid if any formed during the test.

To ensure the most accurate collection and weighing of all phases, the PetroOXY seal, the empty crucible, and the liquid phase collection bottle are initially weighed before the oxidation experiment. Then, the initial mass of *n*-dodecane is weighed directly into the crucible before being introduced into the PetroOXY apparatus. At the end of the oxidation, the liquid phase present in the crucible (as well as the residual liquid present on the lid and the edges of the device) is meticulously recovered with a pasteur pipette, then poured into the recovery flask to be weighed. The loss of liquid during this protocol was measured experimentally and the value is 0.15 g +/- 0.01 g. The seal at the end of the tests is also weighed (0.02 g increase in difference between the seal before and after oxidation is always observed). Finally to ensure the recovery of the solid phase, the empty crucible is also weighed. All weighings are performed with a 10⁻⁴ g precision balance with an

accuracy of 100 μg . As the tests are performed 4 times, it is possible to obtain an average between the deviations of each test to arrive at a relative deviation [85]. For all gasification rates, an error of $< 1\%$ is observed.

The conversion rate of dioxygen has been calculated with the formula:

$$\text{Conversion rate of } O_2 (\%) = \frac{(n_{i,O_2} - n_{f,O_2})}{n_{i,O_2}} \times 100$$

where n_{i,O_2} is the initial quantity (mol) of dioxygen and n_{f,O_2} is the quantity (mol) of dioxygen remaining in the gas phase after the test. n_{f,O_2} is obtained by subtracting the quantity of oxidation gas produced to the total quantity of gaseous molecules at the end of the test.

The volumes of oxygen, introduced and consumed during a test, were determined by means of a calibration carried out to establish a correlation between the volume of gas and the pressure measured at room temperature. From this calibration curve (Figure S.M.1.) and the pressure data provided by the PetroOXY device, it was possible to deduce experimentally the volumes of oxygen introduced into the device and the total volume of gas recovered including the unreacted oxygen and the gaseous products formed after oxidation. The quantitative results of the micro-gas chromatography allowed to measure the amount of gaseous products formed, so by considering the total volume of gas recovered and the volume of gaseous products formed, it was possible to deduce the volume of unreacted oxygen. These volumes were converted into mole number using as an approximation that $22.4 \text{ L} = 1 \text{ mol}$ of oxygen. It was thus possible to determine the conversion rates as well as the mole number consumed of dioxygen. Each test has been carried out 4 times. It was possible to calculate the standard deviation for each test condition (deviation $< 10^{-4} \text{ mol}$) [85].

The conversion rate of *n*-dodecane is calculated using the formula:

$$\text{Conversion rate of } n - \text{dodecane } (\%) = \frac{(n_{i,n-\text{dodecane}} - n_{f,n-\text{dodecane}})}{n_{i,n-\text{dodecane}}} \times 100$$

With $n_{i,n\text{-dodecane}}$, $n_{i,n\text{-dodecane}}$ and $n_{f,n\text{-dodecane}}$, $n_{f,n\text{-dodecane}}$ the quantity (mol) of *n*-dodecane initially introduced and remaining in the liquid phase at the end of the test, respectively.

2.3 Characterization techniques

2.3.1. Fourier Transform Infrared Spectroscopy

The gas and liquid phases were analyzed by Fourier Transformed Infra-Red (FTIR) spectroscopy, using a Frontier spectrometer from Perkin-Elmer. The analysis of the gas phase was carried out in transmission, recording 4 spectra in the 4000 - 1000 cm^{-1} wavelength range, with a scanning speed of 0.2 $\text{cm}\cdot\text{s}^{-1}$ and a resolution of 4 cm^{-1} . For the liquid phase, one drop was deposited on a mono-reflexion diamond and analyzed by Attenuated Total Reflectance (FTIR-ATR) equipped with a MCT detector. The same acquisition parameters as for the gas phase were used except that 5 spectra in the 4000 - 450 cm^{-1} wavelength range were recorded.

2.3.2. Micro-Gas Chromatography

The gas phase was also analyzed by micro-GC. The apparatus, an Agilent 490, is equipped with 3 columns: Al_2O_3 (10 m x 0.32 ID, $T_{\text{column}} = 70\text{ }^\circ\text{C}$, $P = 130\text{ kPa}$), CO_x (1 m x 0.7 ID, $T_{\text{column}} = 80\text{ }^\circ\text{C}$, $P = 150\text{ kPa}$), CP sil-5CB (20 m, $T_{\text{column}} = 50\text{ }^\circ\text{C}$, $P = 150\text{ ka}$) and Thermal Conductivity Detectors (TCD). The analysis was carried out with argon and helium as vector gas. Calibration was made before each test for H_2 , CO, CO_2 , and the hydrocarbon molecules.

2.3.3. Gas Chromatography

The liquid phase was analyzed by Gas Chromatography (GC) using a Varian 3900. This apparatus is equipped with an automatic sampler CP-8410, an injector 1177 split/splitless, a capillary column PONA type, a fused silica capillary column (phase type: VF-5 ms., length: 60 m, internal diameter: 0.25 mm, phase thickness: 1 μm) with a column flow of 0.8 mL/min and a Flame Ionization Detector (FID). The analysis was carried out with helium as the vector gas. The injection temperature is set at 250 $^\circ\text{C}$. The thermal program was optimized for *n*-dodecane: 5 min at 50 $^\circ\text{C}$;

heating up to 175 °C (at a speed of 5 °C.min⁻¹) for 5 min; to 185 °C (2 °C.min⁻¹) for 5 min; to 215 °C (2 °C.min⁻¹) for 5 min, then to 250 °C (2 °C.min⁻¹) for 10 min.

Standards were prepared by mixing different volumes of *n*-dodecane and *n*-decane (purity > 99 %, Alfa Aesar). These standard solutions and the oxidized samples were injected 3 times and a deviation of less than 1 % was imposed.

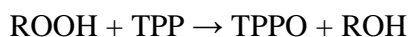
2.3.4. Gas Chromatography/Mass Spectrometry

Identification of the products in the liquid phase was carried out by a Gas Chromatograph coupled to a mass spectrometer (GC/MS) with a Varian 450 GC/320 MS. The same column and thermal program as with the GC Varian 3900 were used. The MS fragmentation was obtained by an electronic impact of 70 eV.

2.4. Quantification of the products formed

2.4.1. Identification of hydroperoxide species

The presence of hydroperoxide species was evidenced through the oxidation of triphenylphosphine (TPP) to the corresponding oxide (TPPO) following the reaction [86, 87]:



To this purpose, 4 g of TPP (99 %, Acros Organics) and 0.3 g of fluorene (> 98 %, Acros Organics) were dissolved in 50 mL of chloroform (≥ 99.8 %, Carl Roth). 250 μL of this solution were added to 1 mL of oxidized *n*-dodecane and stirred for 10 min before analysis by GC and GC/MS. The limit of detection of this method is < 0.002 mM.

2.4.2. Peroxide Value

Peroxide species formed during the test were back titrated using a method close to that described in the ASTM D3703 standard [88], relying on the reduction of the iodide molecules formed during titration with sodium thiosulfate.

The Peroxide Value (PV) was calculated according to the formula [87,89]:

$$PV = ((A-B) N \times 1000)/V$$

where A and B are the volumes of a sodium thiosulfate solution, of normality N, added during the assay and a blank test, respectively, to a volume V of sample.

2.4.3. Total Acid Number (TAN)

The total acid number (TAN) is the mass of KOH needed to neutralize the free acid molecules present in 1 g of sample [68]. The method employed to determine the TAN is based on the ASTM D3242 standard [91]. It is an acido-basic titration, suitable in the range from 0.000 to 0.10 mg KOH/g.

2.4.4. Water Content

The water content was determined by coulometric titration with a Karl-Fisher titrator (Mettler Toledo C30 with a Pt electrode under 20 μ A). The anolyte and catolyte used were the HYDRANAL Coulomat AK and HYDRANAL Coulomat CGK solutions Honeywell Fluka), respectively.

3. RESULTS

3.1 Influence of the reaction progress

3.1.1 Consumption of dioxygen and n-dodecane

The oxidation of *n*-dodecane was first carried out in the PetroOXY device at a temperature and initial pressure set at 160 °C and 700 kPa, respectively, and stopped at different pressure drops, $\Delta P/P_{max}$ from 0 to 10 %. These low reaction progress values were chosen to study the beginning of the autoxidation process.

Figure 1.a) shows the evolution of pressure with the test duration. The first part of the curves corresponds to the increase of pressure associated with heating. When *n*-dodecane is oxidized, the consumption of oxygen results in a decrease of the pressure. Nevertheless, the form of the curves

results from two antagonist phenomenons: the consumption of oxygen and the production of gas. The curves obtained for the different $\Delta P/P_{max}$ are superimposed, proving the reproducibility of the results. Each test condition has been carried out 4 times.

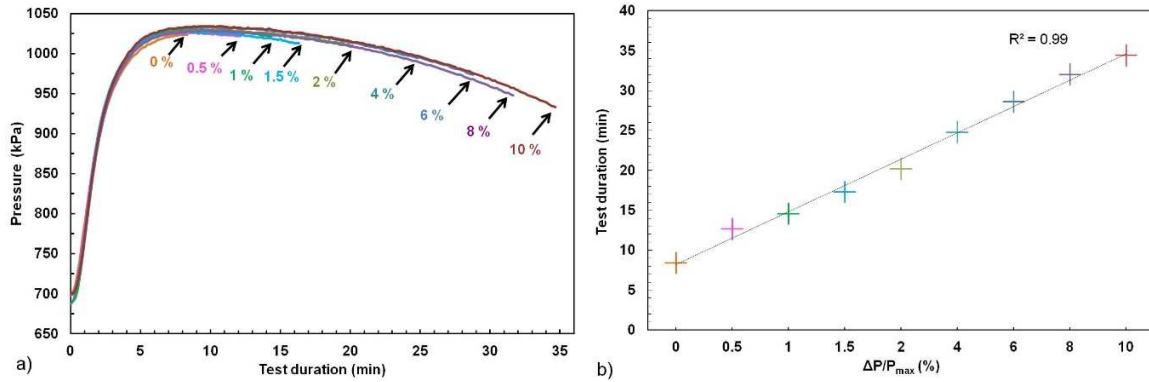


Figure 1. a) Evolution of the pressure with test duration for different $\Delta P/P_{max}$ and b) corresponding evolution of the average duration test plotted as a function of $\Delta P/P_{max}$ ($T_i = 160\text{ }^\circ\text{C}$, $P_{O_2} = 700\text{ kPa}$).

The average of the test duration for each $\Delta P/P_{max}$ targeted is presented in Figure 1.b) and show a linear evolution.

Dioxygen and *n*-dodecane consumptions are plotted as a function of the test duration (Figure 2). They both evolve linearly with $\Delta P/P_{max}$ but the molar consumption of dioxygen is greater than that of *n*-dodecane.

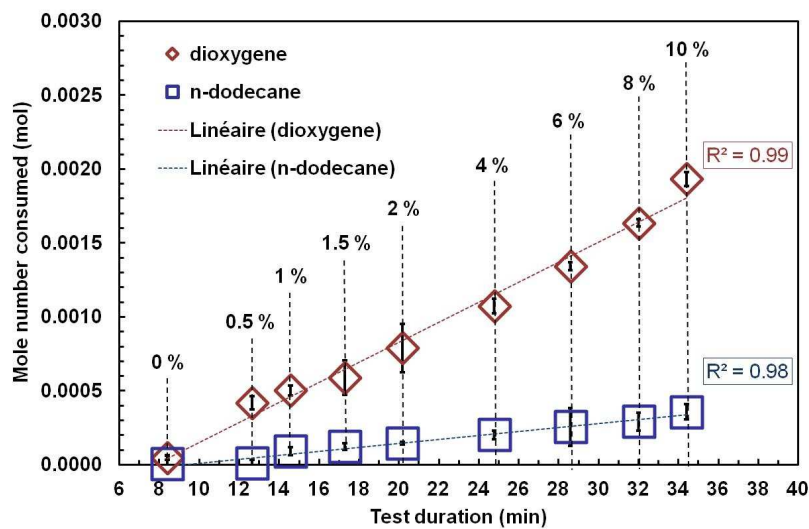


Figure 2. Evolution of oxygen and *n*-dodecane consumption with increasing test duration and $\Delta P/P_{max}$ ($T = 160\text{ }^\circ\text{C}$, $P_{O_2} = 700\text{ kPa}$).

3.1.2 Characterization of the oxidation species formed in the gas phase

At $\Delta P/P_{\max} = 10\%$ the gasification rate measured is around 0.72 %, which implies that the production of gaseous products is rather limited.

The gas products were first analyzed by FTIR spectroscopy. New peaks arise and grow as the reaction proceeds as evidenced by the spectra given in Figure 3. They are characteristic of oxidation products: the bands between 3447 and 3764 cm^{-1} can be attributed to the $\nu_{(\text{O-H})}$ stretching vibration of alcohols and carboxylic acids; the peak at 2737 cm^{-1} is typical of the $\nu_{(\text{C-H})}$ aldehyde stretching vibration, and that at 1740 cm^{-1} corresponds to the $\nu_{(\text{C=O})}$ vibration of ketones, carboxylic acids and aldehydes. The formation of CO is evidenced by the double band at 2112 and 2172 cm^{-1} , characteristic of its $\nu_{(\text{C}\equiv\text{O})}$ stretching vibration. Furthermore, $\nu_{(\text{C-H})}$ vibrations of CH_2 and CH_3 groups emerge at 2865, 2931, 2970, 1453 and 1366 cm^{-1} . They can also be attributed to hydrocarbons and oxidation compounds. Another peak with a low intensity but very thin is observed at 3018 cm^{-1} . It is typical of the $\nu_{(\text{C-H})}$ methane stretching vibration. The intensity of all these peaks increases with reaction time.

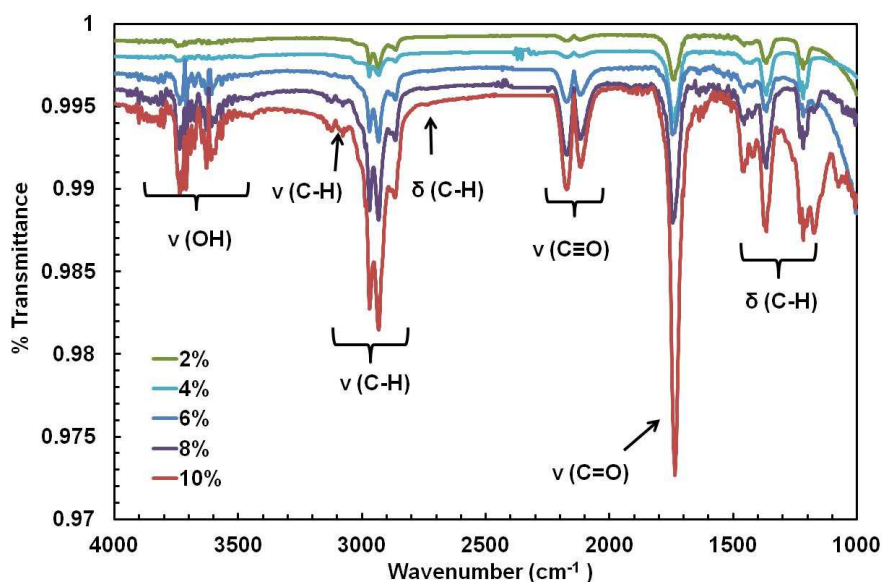


Figure 3. FTIR spectra of the gas phase for different $\Delta P/P_{\max}$ ($T = 160\text{ }^{\circ}\text{C}$, $P_{\text{O}_2} = 700\text{ kPa}$, $\Delta P/P_{\max} = 2$ to 10 %).

The gas phase was further analyzed using micro-GC to identify more specifically the molecules formed. The chromatograms (see Figure SM.2) confirm the production of CO, CO₂, H₂O, H₂ and acetone as already brought out by FTIR at the very beginning. Methanol, ethanol, methane, alkanes and alkenes from C₂ to C₅ are also identified but for $\Delta P/P_{\max}$ values ≥ 4 %. The volumes of these gas species increase with the progress of the reaction as displayed in Figure 4 a) and b), even if they remain low. CO₂ is the gas formed in majority from $\Delta P/P_{\max} = 0.5$ to 10 %. Its quantity increases rapidly. The other identified gases which succeed it in terms of quantity are: H₂, CO, alkenes and alkanes. H₂ and CO are observed at a significant quantity when the reaction reaches $\Delta P/P_{\max} = 2$ % while hydrocarbons are detected only for $\Delta P/P_{\max}$ values ≥ 4 %. The quantity of the alkanes remains lower than that of the alkenes.

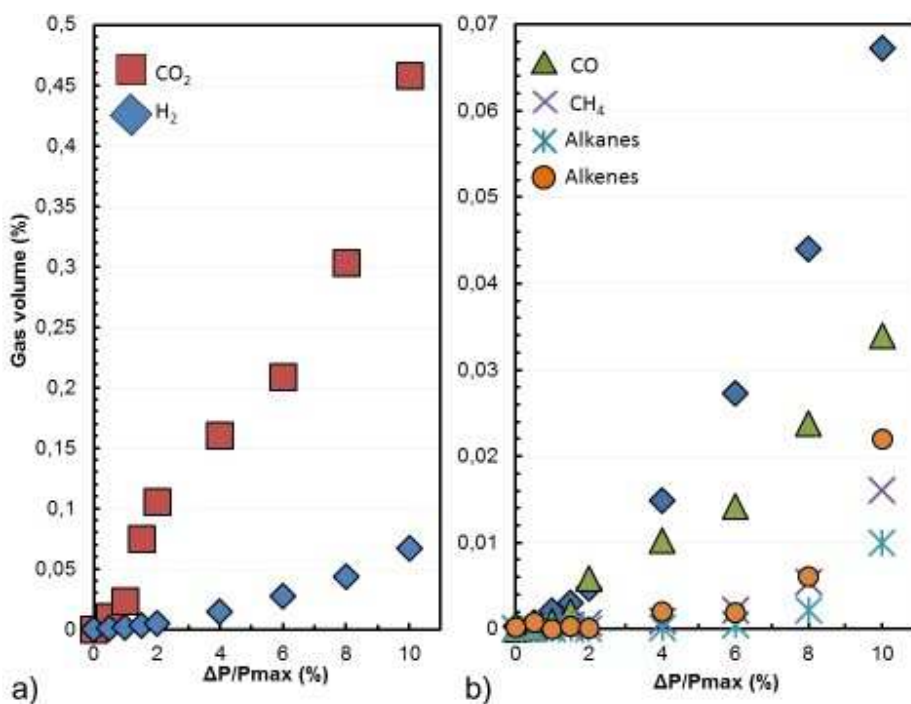


Figure 4. Evolution of the oxidation products determined in the gas phase by micro-GC ($T = 160$ °C, $P_{O_2} = 700$ kPa, $\Delta P/P_{\max} = 0$ to 10 %).

3.1.2. Characterization of the oxidation products formed in the liquid phase

GC-MS was used to characterize the oxidation products of *n*-dodecane in the liquid phase (Figure 5). The products generated during all the oxidation process are identical and their quantity increases with the duration of the test; for the retention times lower than 34 min (Figure 5.a and b) the compounds detected have chain lengths shorter than *n*-dodecane.

It is noteworthy that, in each case, three types of compounds, *i.e.* carboxylic acid, 2-ketone and the corresponding aldehyde, with identical number of carbon atoms are produced. The production of ketones and carboxylic acid species were also evidenced by FTIR (Figure SM.3.1). The molecules with retention times from 42 to 46 min (Figure 5.c) have the same number of carbons as *n*-dodecane. They are alcohols and ketones, *x*-dodecanol and *x*-dodecanone with $x = 1$ to 6, issued from the direct oxidation of *n*-dodecane. These results are similar to that already reported in the literature [59,81]. In addition, dodecanal was identified but dodecanoic acid was not found as it was expected. This could be explained by the fact that its boiling temperature is very high (298 °C) so that this product could not be vaporized and thus injected in the GC. Eventually, peaks at retention times near 53 min (peaks 1 to 6 in Figure 5.d), correspond to m/z 169 are observed. This ratio is characteristic of hydroperoxide species [67] and the 6 peaks are thus probably isomers of dodecyl-hydroperoxide.

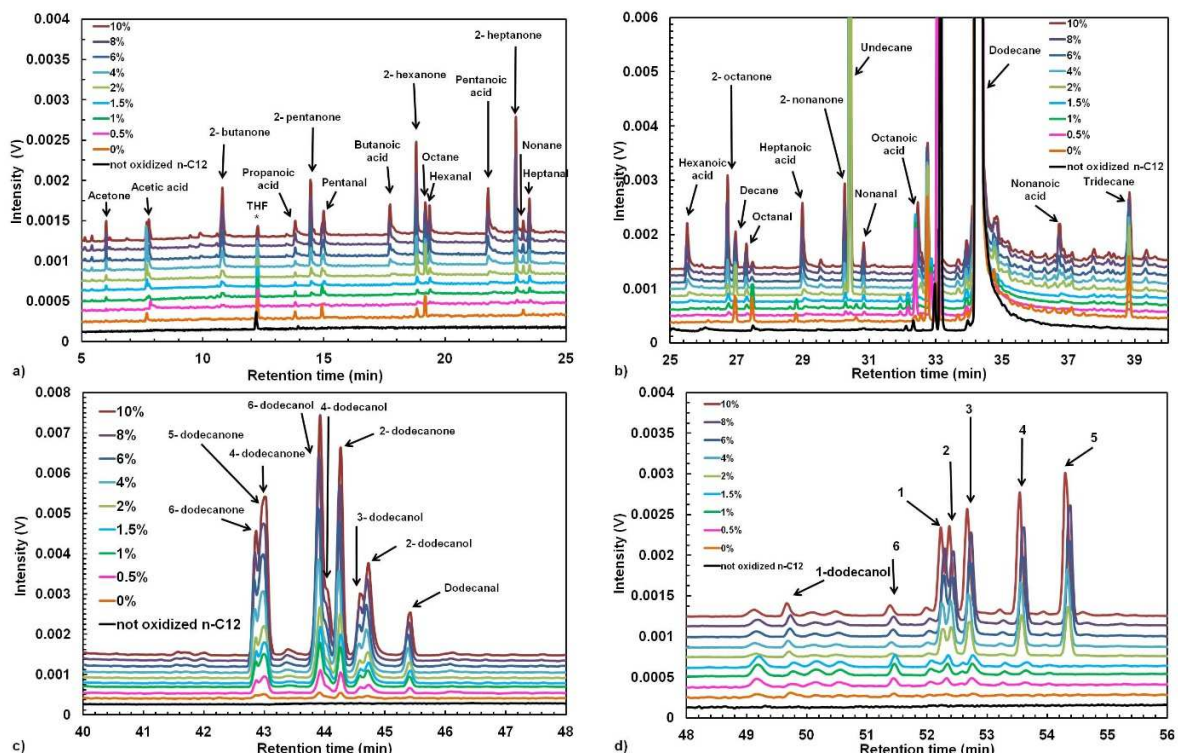


Figure 5. Gas phase chromatograms of the liquid phase for $\Delta P/P_{max} = 0$ to 10 % for four different retention time ranges. Identification of the products was obtained by MS.

To confirm the identification of these hydroperoxides, a back titration, based on their reduction into alcohols in the presence of TPP, was carried out [86,87]. The intensity of the peaks 1 to 6 in Figure 5.d should decrease in intensity while the peaks in Figure 5.c of the corresponding alcohols should increase as the TPP is oxidized into TPPO. This is indeed what is observed in Figure SM.3.2, confirming the attribution of the peaks of retention time from 50 to 55 min. to x-dodecyl-hydroperoxides.

Quantitative GC analysis requires the use of standards. During the oxidation of the *n*-dodecane, so many products are formed that it is not possible to calibrate all of them. However, semi-quantitative analysis can be carried out by comparing the surface area of the peaks. The cumulative surface area of each family of compounds was calculated and plotted in Figure 6 for increasing $\Delta P/P_{max}$. The quantity of primary (hydroperoxides) as well as the secondary (alcohols, ketones,

carboxylic acids...) oxidation products increases with $\Delta P/P_{max}$. The major products are ketones, then hydroperoxides.

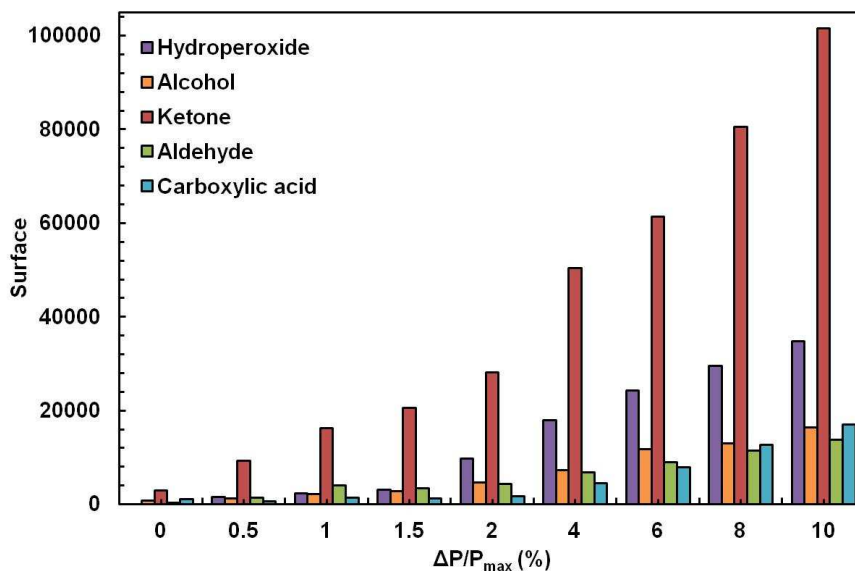


Figure 6. Evolution of the products generated during the oxidation of *n*-dodecane as a function of $\Delta P/P_{max}$ obtained by GC.

To confirm the GC results, chemical titration was also carried out. The peroxide value, PV, Total Acid Number, TAN, related to the amount of carboxylic acids formed including dodecanoic acid, and water content are plotted in Figure 7. Their evolutions are linear and consistent with that observed by GC (Figure 6).

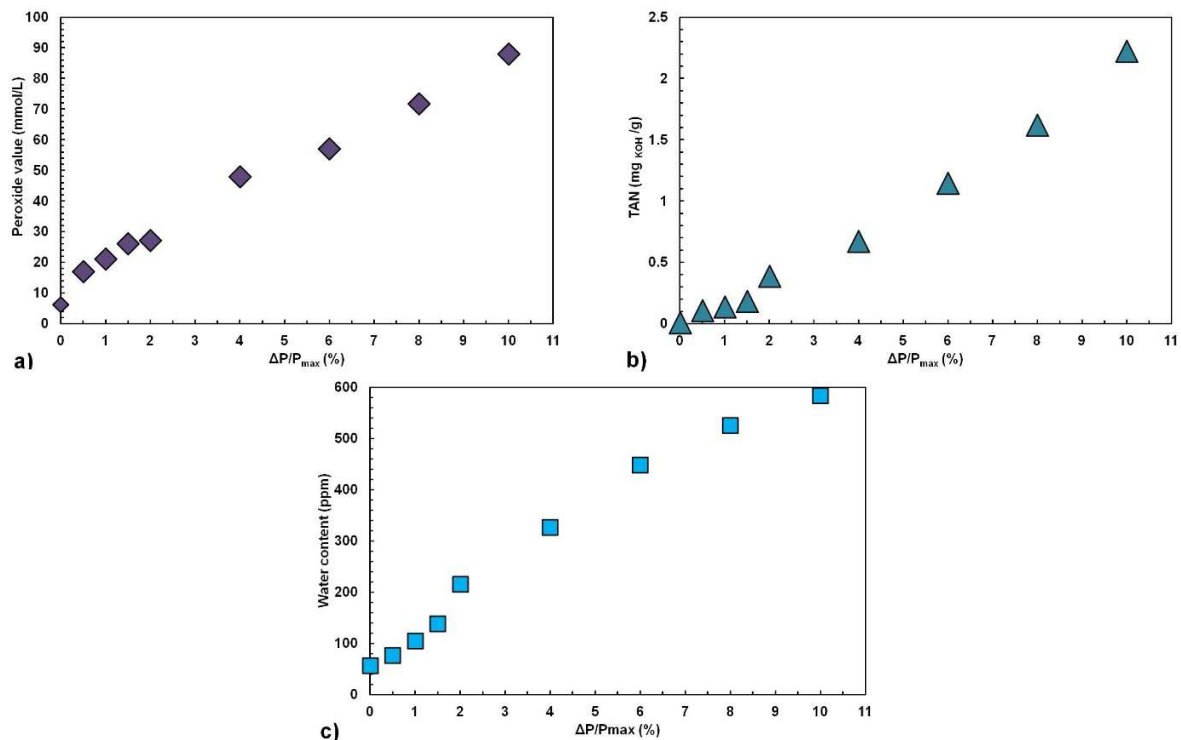


Figure 7. Evolution, deduced from GC measurements, in the liquid phase of a) the Peroxide Value, b) TAN and c) quantity of water with increasing $\Delta P/P_{max}$ ($T = 160$ °C, $P_{O_2} = 700$ kPa).

Linear plots of concentration versus time demonstrate zeroth order kinetics. It is well known that oxidation proceeds via zeroth order (at high initial oxygen levels) initially, but it's interesting to observe these reaction products are being produced under similar zeroth order kinetic.

3.2. Influence of the temperature

3.2.1 Dioxygen and n-dodecane conversions

In the second set of experiments, $\Delta P/P_{max}$ was fixed at 10 % with the same initial pressure of dioxygen of 700 kPa as previously, but three temperatures were targeted: 140, 150 and 160 °C. The evolution of the pressure for the three temperatures is plotted in Figure 8. All the curves have similar shapes but the time to reach the targeted $\Delta P/P_{max}$ decreases with increasing temperature.

The induction periods, deduced from these curves, are given in Figure S.M.4.1. The values confirm that increasing the temperature accelerates the oxidation reactions.

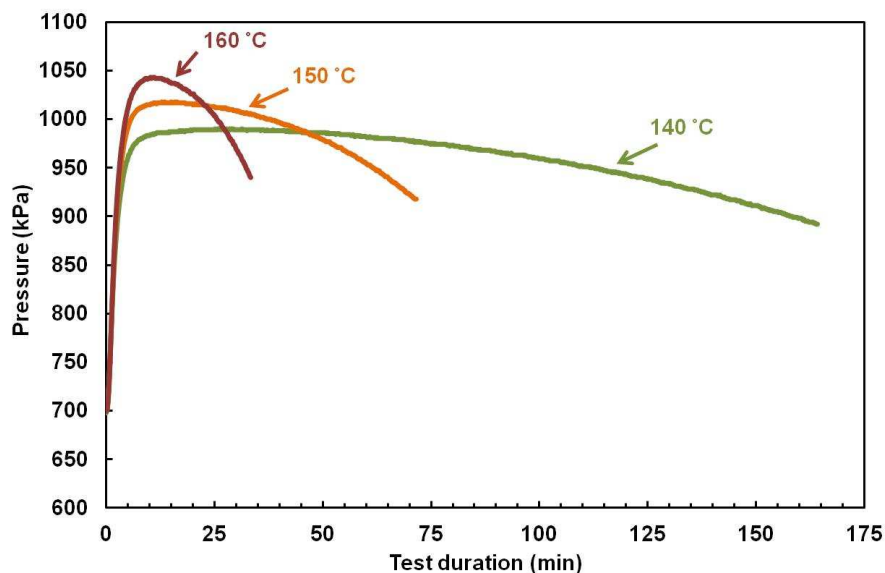


Figure 8. Evolution of the pressure with duration time for three different temperatures ($P_{O_2} = 700$ kPa, $\Delta P/P_{max} = 10\%$).

As previously stated, the evolution of the oxidation reaction was followed using the gasification rate and the dioxygen and *n*-dodecane conversions. These values are plotted for the three considered temperatures in Figure S.M.4.2. The gasification rates are similar whatever the temperature is and they are less than 0.7 %. The consumption of dioxygen increases with the temperature from 18 to 23 % while the *n*-dodecane conversion remains low with an increase from 1.0 to 1.6 %.

3.2.2 Characterization of the gas and the liquid phases

The results of FTIR spectroscopy and micro-GC show similar oxidation products in the gas phase whatever the temperature is. CO₂ is always the product formed in majority and its quantity, in proportion by comparison to other molecules, increases significantly when the temperature goes from 140 to 160 °C. At 140 and 150 °C, the proportions of CH₄, alkanes and alkenes formed are

equivalent, but that of alkenes increases significantly at 160 °C. The amounts of H₂ and CO remain globally constant (Figure 9.a).

The liquid phase was characterized by FTIR and GC/MS. These techniques evidence the same oxidation products whatever the temperature is. Their quantitative evolution, given in Figure 9.b, shows an increase of all the oxidation species with increasing temperature but the ratios of the products to each other remain equivalent. The major products are ketones, followed by hydroperoxides. The peroxide value, the water content and the acid number were also measured. The results are shown in Figure S.M.4.3. They show a linear increase of all these values with temperature.

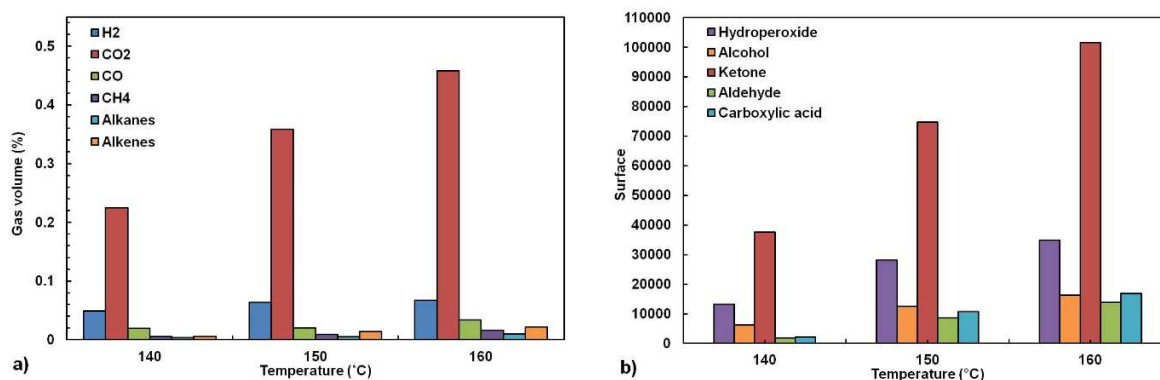


Figure 9. Evolution of the a) volume of the different oxidation products in the gas phase, obtained by micro-GC, and b) oxidation products in the liquid phase determined by GC, for three different temperatures ($\Delta P/P_{max} = 10\%$, $P_{O_2} = 700$ kPa).

4. DISCUSSION

4.1. Impact of temperature on n-dodecane and dioxygen consumptions

The monitoring of the consumption of n-dodecane and dioxygen at 160 °C and 700 kPa presented in Figure 2 shows a linear evolution of each of the reactants, indicating a constant consumption rate regardless of the reaction advancement ($\Delta P/P_{max} = 0$ to 10%). The consumption of these two reactants is equivalent at the start ($\Delta P/P_{max} = 0\%$): 0.0049 mmol of dioxygen and 0.0047 mmol of n-dodecane. Then, the consumption of dioxygen increases more rapidly than that

of *n*-dodecane to a five-fold increase at $\Delta P/P_{\max} = 10\%$. This can be justified by the fact that initially, at $\Delta P/P_{\max} = 0\%$, dioxygen could only react with *n*-dodecane, the only reactant present, and subsequently these two molecules react together to form a hydroperoxide. But very quickly, other competing reactions appear and consume also the dioxygen. Thus, for the value of $\Delta P/P_{\max} = 10\%$, the ratio moles $O_2/n\text{-}C_{12}H_{26}$ consumed is about 5/1.

A clear influence of the temperature on the induction period is evidenced. As expected, the higher the temperature is, the shorter the induction period is. As a reminder, $\Delta P/P_{\max}$ is directly linked to the consumption of dioxygen. Thus, the temperature accelerates the speed of consumption of dioxygen, which increases from 8.8×10^{-3} mmol/min at 140 °C to 5.5×10^{-2} mmol/min at 160 °C. Nevertheless, it is not possible to compare directly the induction periods as done in previous works [71,77,81-83]. Indeed, at a fixed $\Delta P/P_{\max}$, the quantitative analysis carried out in this study evidences that the conversions of dioxygen are not identical: they are 0.015 and 0.018 mmol at 140 and 160 °C, respectively. Due to the difference of temperature, the P_{\max} obtained in the batch system is not the same. This has an impact on the calculation of the ΔP and, as a consequence, on the level of dioxygen consumption.

Consequently, to highlight the real impact of temperature, the tests would have been carried out at iso-conversion of the dioxygen (same consumption of dioxygen) and not at the same $\Delta P/P_{\max}$. It was rather easy to estimate the additional time needed with the dioxygen speed consumption, expressed in mmol/s, calculated previously. Thus, this hypothesis was confirmed by carrying out tests with the corrected induction periods and iso-conversion of dioxygen was obtained as shown in Figure S.M.5. The corrected IP presented in Table 1 will be used later in the kinetic study.

Table 1. IPs results obtained experimentally at $\Delta P/P_{\max} = 10\%$ and after correction ($P_{O_2} = 700\text{ kPa}$).

Temperature (°C)	140	150	160
Experimental IP (min)	169	71	33
Corrected IP (min)	208	78	33

4.2 Formation of oxidized products

After the oxidation tests under the conditions studied, i.e. $\Delta P/P_{\max} = 0\text{-}10\%$, $T = 140\text{-}160\text{ }^\circ\text{C}$ and $P_{O_2} = 700\text{ kPa}$, the characterization of the gas phase revealed that CO_2 is mostly produced, followed by H_2 , CO , CH_4 , alkenes and then alkanes, as well as other polar molecules, such as water, methanol, ethanol and acetone. Furthermore, the products detected in the liquid phase are hydroperoxydes, primary and secondary alcohols, ketones, aldehydes, carboxylic acids and water.

All the products formed are identical and their quantity increases with either increasing $\Delta P/P_{\max}$ or temperature. But the quantities of hydroperoxides, ketones and carboxylic acids increase more rapidly than other products. This could highlight an effect of accumulation of these products and could be explained by kinetics of transformation from alcohols to ketones or to carboxylic acids faster than for the reactions from hydroperoxides to alcohols. Thus, it is possible to divide all the products into three classes:

- the hydroperoxides;
- the oxidized products with a carbon chain with 12 atoms as the parent molecule;
- the other products with a shorter carbon chain.

In this study, the hydroperoxides produced from *n*-dodecane have been characterized. The six isomers of the dodecyl-hydroperoxide were identified, indicating that the formation of the alkyl radical $\text{R}\cdot$ is possible along the whole *n*-dodecane hydrocarbon chain. Their quantity increases

linearly with the reaction time and never reaches a plateau. This points out that their production rate is higher than their consumption rate, at least up to $\Delta P/P_{\max} = 10\%$.

The second category of oxidized products gathers the molecules having the same carbon chain length as the *n*-dodecane. The ROOH hydroperoxides decompose into RO• and OH• radicals. Then these species will react with the other molecules to form alcohols and water. The formation mechanism will be described later. Six hydroperoxide isomers were formed, five of them will lead to the formation of secondary alcohols and then ketones. This is confirmed on the chromatograms as the five ketone isomers are observed. The sixth one, formed by the attack of hydrogen at the chain end, will lead to a primary alcohol, an aldehyde and then to a carboxylic acid. The dodecanoic acid is not present on the chromatograms, however it is suspected to be in the liquid phase.

The amount of secondary alcohols is found higher than that of the primary alcohols as evidenced in Table 2. It is interesting to note that the area ratio of the primary to secondary alcohols does not vary much with the reaction temperature. Theoretically, if the probabilities of formation of every alkyl radicals from the *n*-dodecane are equivalent, 1/6 of the total alcohols produced should be primary and 5/6 secondary alcohols. Thus, the expected primary to secondary alcohols area ratios should be 0.20; the experimental values obtained are very close, between 0.16 and 0.18.

Table 2. Ratio values of the surface areas obtained by GC for primary and secondary dodecanols in the liquid phase ($\Delta P/P_{\max} = 10\%$, $P_{O_2} = 700\text{ kPa}$).

Temperature (°C)	140	150	160
Area ratio = $\frac{\text{surface of primary alcohol}}{\sum \text{surfaces of secondary alcohols}}$	0.16	0.17	0.18

Some of the oxidized products have a shorter carbon chain than the parent hydrocarbon. Their formations are induced by the breakage of the carbon chain of the *n*-dodecane. In the liquid

chromatograms, alkanes, ketones, aldehydes and carboxylic acids are observed with all the possible carbon chain lengths below 12 carbon atoms. The gaseous products also come from the breakage of the *n*-dodecane carbon chain.

It should be noted that the mechanisms presented in the literature highlight other secondary products resulting from the autoxidation of *n*-dodecane, such as esters, ethers, epoxides, lactones, diones and furanones [18,28,39,59,81]. In these studies, the fuels have been oxidized for longer times and sometimes at temperatures above 160 °C. In this study, it was not possible to find these products in the liquid phase.

4.3 Autoxidation mechanism

Based on the mechanisms proposed in the literature and our experimental results, we attempted to establish the reaction scheme of the *n*-dodecane oxidation.

Hydroperoxides formation

If we use the mechanism proposed by Heneghan and Zabanick [47], the hydroperoxides are the first oxidized products. They are formed according to these two reactions:



The first step consists in a quick reaction of the alkyl radical $R\bullet$ with a molecule of dioxygen to form an alkyl peroxide radical $RO_2\bullet$. Then, the latter takes a hydrogen atom from *n*-dodecane to form a ROOH hydroperoxide and regenerate an alkyl radical $R\bullet$. The new carbon radical formed can then react with dioxygen to continue the cycle.

Oxidized products with a 12 atoms carbon chain

The dissociation of the hydroperoxide molecule is obtained by a scission reaction [46], leading to the formation of two radicals, alkoxy and hydroxyl, according to the following reaction:



The alkoxy radicals can take a hydrogen atom from *n*-dodecane as follows:



This mechanism is in agreement with the results obtained insofar as it allows explaining the decomposition of hydroperoxides into primary and secondary alcohols as well as the formation of water. Then, the primary and secondary dodecanol molecules would oxidize into dodecanone and dodecanal, respectively. Two mechanisms can be proposed (Figure 10 illustrates the transformation of 6-dodecanol into 6-dodecanone). The first step is an intermolecular abstraction reaction involving the hydrogen atom of the alcohol group of dodecanol with another alkyl radical $\text{R}\cdot$, leading to a $\text{RO}\cdot$ radical. The second step can consist either in a second intermolecular reaction between the $\text{RO}\cdot$ radical and alkyl radical species $\text{R}\cdot$ followed by a rearrangement reaction (on the left) or an intermolecular abstraction reaction between an $\text{OH}\cdot$ radical which will interact with the hydrogen of the carbon carrying the $\text{CO}\cdot$ bond (on the right).

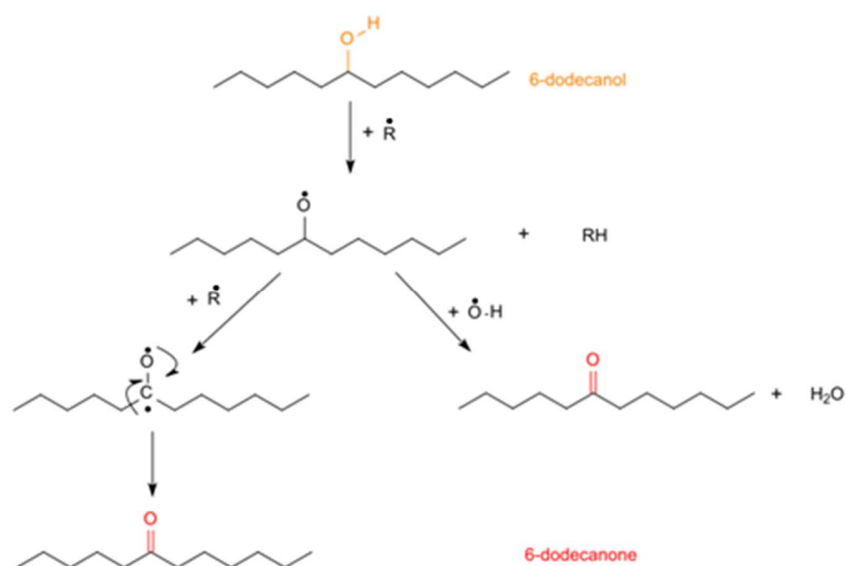


Figure 10. Formation mechanisms of the 6- dodecanone.

The dodecanoic acid comes from the oxidation of the dodecanal [18]. Thus, the latter would undergo a hydrogen abstraction reaction, thus forming a carbonyl radical $\bullet\text{R}=\text{O}$. On the latter is added a dioxygen atom, to form an $\text{R}(\text{O})\text{OO}\bullet$ radical. It is stabilized by stripping a hydrogen atom from a RH species to form $\text{R}(\text{O})\text{OOH}$. Once stabilized, successive rearrangement reactions will take place, thus forming a carboxylic acid.

Oxidized products with a chain with less than 12 carbon atoms

The experimental results also demonstrated the presence of molecules of 2-ketones, aldehydes and carboxylic acids with less than 12 carbon atoms (Figure 5). To explain their formation, one must take into account the possibility of obtaining all carbon chain lengths shorter than that of n-dodecane, and not involving the production of alcohol molecules. This suggests a very different mechanism from the ones proposed to explain the formation of dodecanone molecules and dodecanoic acid.

The mechanisms presented in Figure 11 are inspired from the octane combustion mechanism proposed by Sarathy et al. [92] for temperatures below 477 °C (750 K). In this mechanism, a dioxygen molecule reacts with an *n*-dodecane alkyl radical to form a hydroperoxide radical $\text{ROO}\bullet$. This hydroperoxide radical can undergo intramolecular isomerizations inducing the formation of a six-membered ring to form a QOOH radical. This radical is reactive and can form, by reacting with an oxygen molecule, a radical $\bullet\text{OOQOOH}$. The latter will undergo a second six-membered intramolecular isomerization to tear off the hydrogen atom present on the carbon bearing the OOH group since this C-H bond is weaker. Removal of the hydrogen atom will induce the formation of a free radical $\text{HOO}\bullet$ QOOH molecule [93]. This radical will subsequently decompose by β -scission reactions [94] thus forming a keto-hydroperoxide (KHP) species with the elimination of an $\text{OH}\bullet$ radical. The KHP species formed will then quickly break down into smaller molecules by β -

scission reactions on the OOH group, inducing the elimination of another OH• radical as well as the formation of two molecules: a 2-ketone and an aldehyde type molecule found in the liquid and gaseous phases [95,97].

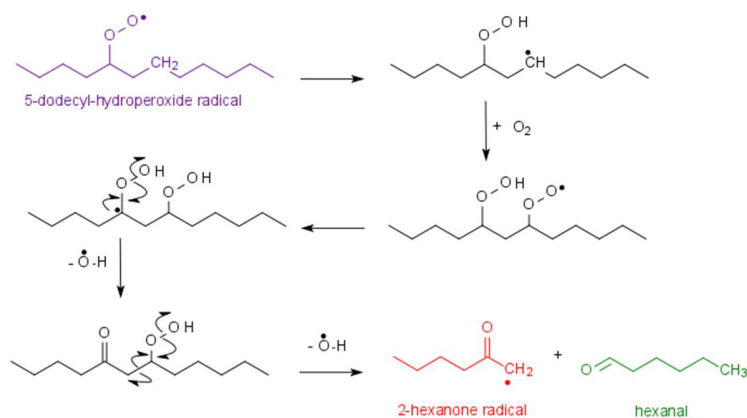


Figure 11. Formation mechanism of ketones and aldehydes.

The short carboxylic acids can be formed *via* the same mechanism used to explain the formation of the dodecanoic acid. Nevertheless, the Korcek's reaction is an alternative interesting path [40,79,98]. This involves an intramolecular reaction of the KHP molecule, forming a 5-membered ring leading to a carboxylic acid and an aldehyde and/or a ketone (Figure 12).

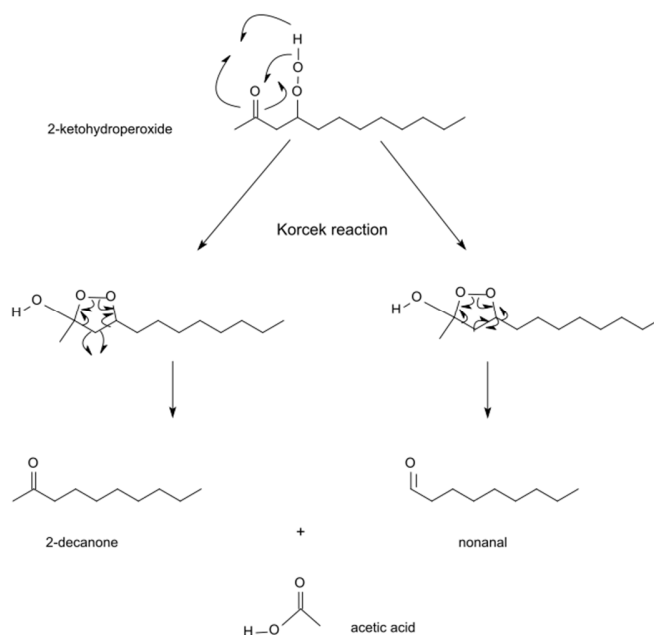


Figure 12. Ketones, aldehydes, carboxyl acids formation by the Korcek's mechanism.

Formation of water

The radical $\text{OH}\cdot$ is often produced in the mechanisms proposed previously: the decomposition of the hydroperoxides, the oxidation of dodecanol into dodecanone and of dodecanal into dodecanoic acid, the formation of the shorter oxidized products (Figure 11). It is assumed that water is formed after hydrogen abstraction from *n*-dodecane.

Formation of carbon monoxide and dioxide

As mentioned above, whatever the experimental conditions are, the predominant oxidation product in the gas phase is CO_2 . A decarboxylation reaction can explain its formation. It could take place during the formation of the carboxylic acid. The carboxyl radicals can expel a carbon dioxide to produce an alkane radical.

Likewise, CO can be formed during the production of the short aldehydes. Indeed, when the aldehyde is produced, an $\text{OH}\cdot$ radical is also present and could easily tear off the hydrogen in alpha

position and form an acyl radical. This latter would decompose to form an alkyl radical and a carbon monoxide molecule.

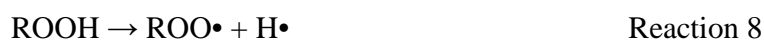
Formation of dihydrogen

H₂ is significantly detected from $\Delta P/P_{\max}$ values $\geq 4\%$ (Figure 4). It could result from the decomposition of an alkyl radical as follows:



This reaction is interesting because it explains also the formation of the alkenes.

Another hypothesis could be the decomposition of a hydroperoxyde following the reactions:



According to the results of the current study, the mechanism of formation of H₂ is inconclusive. Based on the quantitative analysis of the gas phase, it is important to keep in mind that H₂ is formed in very small quantities. However, based on all of the above assumptions (Reactions 8 to 11), it is possible at a further stage to consider studies to determine its formation mechanism.

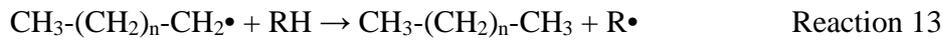
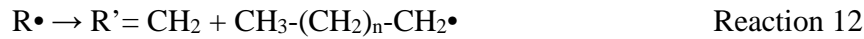
Formation of methane, alkanes and alkenes

Another hydrocarbon found in the gas phase is methane. To produce this molecule, a radical CH₃• should be an intermediate species. According to the literature [47,48], it results from the unimolecular scission of the larger alkyl radicals which react to form a methyl radical and an alkene as follows:



This reaction is another way to obtain the alkene molecules.

Similarly, short alkanes and alkenes could be formed by the same β -scission reaction:



4.4 Kinetic study

Global reaction rate constant

Based on the mechanism proposed by Heneghan and Zabarnick [47], Bacha *et al.* [77] established kinetic equations fitting with the test conditions of the PetroOxy. They allow determining the global kinetic rate constant k of the oxidation reaction and, based on a simplified hydrocarbon oxidation mechanism (Heneghan and Zabarnick [47]), and assuming that this constant follows the Arrhenius formalism, calculating the activation energy E_a and the pre-exponential factor A .

To calculate the constant k , the authors made some approximations. They assumed that:

- the conversions of dioxygen and hydrocarbons were equivalent for the reactions at $\Delta P/P_{max} = 10\%$ whatever the temperature is;
- they determined the mole fraction of dioxygen consumed during the induction period by considering the initial and final dioxygen mole numbers from the ideal gas law;
- they approximated the molar fraction of fuel consumed during the induction period to be 95 % of the initial molar fraction of fuel.

In this work, the mechanism and the analysis of Bacha *et al.* [77] were used to determine the overall reaction rate parameters. However, unlike the study by Bacha *et al.*, in the current study no approximation was made to determine the mole fraction consumed during the induction period of dioxygen and fuel data, i.e., the overall reaction rate parameters for calculating the k constant were determined experimentally. Moreover, these authors [77] take into account the experimental induction periods, but it was shown in this study that it was necessary to be at iso conversion of

the reagents and therefore to consider the corrected induction times (Table 1). Thus, their equation was modified to take into account these new elements:

$$\ln \left[\frac{\Delta n(O_2)}{\Delta n(nC_{12}H_{26})IP} \right] = -\frac{E_a}{RT} + \ln A \quad \text{Equation 1}$$

with $\Delta n(O_2)$ and $\Delta n(C_{12}H_{26})$ the numbers of moles of dioxygen and *n*-dodecane consumed respectively, IP is expressed in seconds.

The corrected induction periods (Table 1) were plotted as a function of 1/T. A straight line was obtained by linear regression (Figure S.M.6), allowing to determine the values: $E_a = 128.79$ kJ.mol⁻¹ and $A = 2.86 \times 10^{+12}$ s⁻¹. The back calculated rate constants of the oxidation reaction of *n*-dodecane presented in

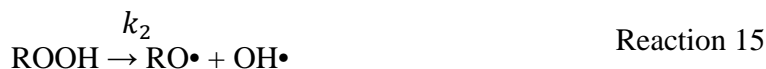
Table 3 for each test temperature were then deduced by using Arrhenius regression estimates.

Table 3. Kinetic constants (k) of n-dodecane oxidation determined using Arrhenius regression estimates ($E_a = 128.79$ kJ.mol⁻¹ and $A = 2.86 \cdot 10^{+12}$ kJ.mol⁻¹).

Temperature (°C)	140	150	160
k (s⁻¹)	1.49×10^{-4}	3.61×10^{-4}	8.39×10^{-4}

Hydroperoxide dissociation rate constant

The literature data and experimental results in this present study suggest that oxidation products result from the formation and decomposition of hydroperoxyde products, as illustrated by the following reactions:



From the two previous reactions, it is possible to establish the evolution of the hydroperoxide's concentration as a function of time during the oxidation reaction:

$$d \frac{[RO_2H]}{dt} = k_1[RO_2 \cdot][RH] - k_2[ROOH] \quad \text{Equation 2}$$

The ROOH concentration is determined with the PV peroxide value measured experimentally for each temperature (Table 4).

Moreover, according to the literature [77], the consumption of dioxygen can be expressed by the relation:

$$- \frac{d[O_2]}{dt} = k_1[RO_2 \cdot][RH] \quad \text{Equation 3}$$

where the kinetic constant k, previously determined (Table 3) can be associated to:

$$k = k_1[RO_2 \cdot] = A e^{-\frac{E_a}{RT}} \quad \text{Equation 4}$$

By injecting the kinetic constant k into the Equation 2 and integrating it between t = 0 and t = IP, one obtains:

$$\frac{d[RO_2H]}{dt} = k \int_0^{IP} [RH] - k_2 \int_0^{IP} [RO_2H] \quad \text{Equation 5}$$

By using the experimental data, it is possible to determine the kinetic constant k₂, by the following relation (Equation 6):

$$k_2 = k \frac{([RH]_{IP} - [RH]_0)}{[RO_2H]_{IP}} - \left(\frac{1}{IP}\right) \quad \text{Equation 6}$$

The kinetic constant of the hydroperoxide dissociation k₂ obtained for each temperature tested are shown in Table 4.

Table 4. Kinetic constants (k₂) of the hydroperoxide dissociation during n-dodecane oxidation determined using Arrhenius regression estimates (E_a = 86.79 kJ.mol⁻¹ and A = 2.9 × 10⁺⁷ s⁻¹) and the peroxide values (PV).

Temperature (°C)	140	150	160
PV (mEq/ dm ³)	58.53	72.75	86.76
k ₂ (s ⁻¹)	3.10 × 10 ⁻⁴	5.50 × 10 ⁻⁴	9.96 × 10 ⁻⁴

From the kinetic constant of dissociation of the hydroperoxide obtained for each tested temperature (Table 4) and the formalism of the Arrhenius law it was possible to plot $\ln(k_2)$ as a function of $1/T$. (Figure S.M.7)

The global reaction rate constant k was expected to be slower than the hydroperoxide dissociation rate constant k_2 . This has been confirmed experimentally.

Finally, it was possible to compare the value of the constant k_2 obtained in this work with those in the literature (Table 5). But it is difficult to conclude anything insofar as the values in the literature are mainly average or estimated values for modelling purposes and are already widely dispersed.

With the exception of West (2011) [49], Thomas (1955) [99] and Emanuel' (2013) [100], the differences found between the Arrhenius parameters reported in the literature are generally higher, i.e., double, than those obtained experimentally in this study.

Indeed, the values in other studies [9,20,22,51] were specifically obtained for modelling a kerosene which contains various hydrocarbon families and also antioxidant species. Thus, the discrepancies obtained may be due to the presence of these compounds. In the case of our study, only one hydrocarbon is oxidized.

Also, it should be noted that the temperature range studied in this experimental work is relatively narrow (140 to 160 °C). Ideally, a wider temperature range should have been investigated to limit uncertainties. However, the values obtained for each test condition are significantly different and reproducible. This gives good confidence in the results. To go further and confirm them, it would be interesting to carry out the protocol established in this study at higher temperatures, using other devices, e.g., the RapidOXY.

Table 5. Comparison of the kinetic constants of the hydroperoxide dissociation reaction obtained in this study and in the literature.

ROOH \rightarrow RO \cdot + OH \cdot			
Literature data	A (s ⁻¹)	Ea (kJ/mol)	Kind of study
In this study	$2.9 \times 10^{+7}$	86.8	Experimental
Thomas (1955) [99]	$1.0 \times 10^{+10}$	112,5	Experimental
Emanuel' (2013) [100]	$8.0 \times 10^{+11}$	129.7	Experimental
Ervin <i>et al.</i> (1998) [9]	$1.0 \times 10^{+15}$	154.80	Numerical
Zabarnick (1998) [20], Kuprowicz <i>et al.</i> (2004)[22]	$1.0 \times 10^{+15}$	175.7	Experimental/Numerical, Numerical
Kuprowicz <i>et al.</i> (2007) [51]	$1.0 \times 10^{+15}$	163.2	Numerical
West (2011) [49]	$2.0 \times 10^{+8}$	104.6	Numerical

4. CONCLUSION

The article proposes a robust operating mode for the study of the autoxidation mechanism of hydrocarbons using the PetroOXY device. Hence, a full characterization of all the products formed at low advancement values ($\Delta P/P_{max} = 0$ to 10 %) of n-dodecane is presented.

At the very beginning of the reaction, the rates of consumption of n-dodecane and oxygen are equivalent: they react with each other to form a hydroperoxide. But very quickly, other reactions in competition appear and also consume oxygen, resulting in higher molar consumption of O₂ than the hydrocarbon. In addition, the oxidation products formed in the liquid phase, and for the first time in the gas phase, were identified and quantified with several techniques. They were classified into 3 classes: (i) hydroperoxides, resulting from the first step of oxidation; (ii) oxidized products with a carbon chain with 12 atoms as the n-dodecane; (iii) other products with a shorter carbon chain, coming from the breakage of the n-dodecane carbon chain.

Since the PetroOXY device is a closed system, temperature has a direct impact on the pressure and thus on the calculated induction period. Thanks to the dioxygen consumption speed measured,

it was possible, for the first time, to correct the t_{IP} values that have been further used for the kinetics calculations. Consequently, the global kinetic constant of the reaction oxidation was calculated with a modified equation that takes into account all the experimental parameters, i.e., the molar fraction consumed of dioxygen and n-dodecane with induction period corrected). Moreover, a calculation has also been proposed for the dissociation rate constant of hydroperoxides.

The approach proposed in this work can be applied to the different families of hydrocarbons constituting the kerosene to determine the O_2 /hydrocarbon consumption ratio, the oxidation mechanisms and kinetic constants for these molecules. All these results will be presented in a following article.

REFERENCES

- [1] Balster W. J., Jones E. G., *Effects of Temperature on Formation of Insolubles in Aviation Fuels*, Journal of Engineering for Gas Turbines and Power, 1998, 120, 289-293.
- [2] Heneghan S.P., Schulz W., *Static Test of Jet Fuel Thermal and Oxidative Stability*, Journal of Propulsion and Power, 1993, 9, 1, 5-9.
- [3] Jones E.G., Balster L.M., Balster W. J., *Thermal Stability of Jet-A Fuel Blends*, Energy & Fuels, 1996, 10, 509-515.
- [4] Dahlin K.E., Daniel S.R., Worstell J.H., *Deposit formation in liquid fuels. 1. Effect of coal-derived Lewis bases on storage stability of Jet A turbine fuel*, Fuel, 1981, 60, 477-480.
- [5] Jones L.Hazlett R.N., Li N.C., Ge J., *Storage stability studies of fuels derived from shale and petroleum*, Fuel, 1984, 63, 1152 – 1156.
- [6] Ervin J. S., Williams T. F. , *Dissolved Oxygen Concentration and Jet Fuel Deposition*, Ind. Eng. Chem. Res. 1996, 35, 899-904.
- [7] Jones E. G., *Autoxidation of Aviation Fuels in Heated Tubes: Surface Effects*, Energy & Fuels 1996, 10, 831-836.
- [8] Jones E. G., Balster L.M., Balster W.J., *Autoxidation of Neat and Blended Aviation Fuels*, Energy & Fuels, 1998, 12, 990-995.
- [9] Ervin J. S., Zabarnick S., *Computational Fluid Dynamics Simulations of Jet Fuel Oxidation Incorporating Pseudo-Detailed Chemical Kinetics*, Energy & Fuels, 1998, 12, 344-352.

- [10] Grinstead B., Zabarnick, S., *Studies of Jet Fuel Thermal Stability, Oxidation, and Additives Using an Isothermal Oxidation Apparatus Equipped with an Oxygen Sensor*, Energy & Fuels, 1999, 13, 756-760.
- [11] Pei X-Y, Hou L-Y., *Effect of dissolved oxygen concentration on coke deposition of kerosene*, Fuel Processing Technology, 2016, 142, 86–91.
- [12] Wilson D. I., Watkinson A. P., *Chemical Reaction Fouling: A Review*, Experimental Thermal and Fluid Science, 1997, 14, 361-374.
- [13] Alborzi E., Blakey S., Ghadbeigi H., Pinna C., *Prediction of growth of jet fuel autoxidative deposits at inner surface of areplicated jet engine burner feed arm*, Fuel, 2018, 214 , 528–537.
- [14] Roan M.A., Boehman A.L., *The effect of fuel composition and dissolved oxygen on deposit formation from potential JP-900 basestocks*, Energy & Fuels, 2004, 18, 835–843.
- [15] Heneghan S., Zabarnick S., *The effects of dissolved oxygen concentration, fractional oxygen consumption, and additives on JP-8 thermal stability*, Journal Eng. Gas Turbines Power, 1997, 119, 822–829.
- [16] Liu G., Cao Y., Jiang R., Wang L., Zhang X., Mi Z., *Oxidative desulfurization of jet fuels and its impact on thermal-oxidative stability*, Energy & Fuels, 2009, 23, 5978–5985.
- [17] DeWitt M.J., West Z., Zabarnick S., Shafer L., Striebich R. , Higgins A., Edwards T., *Effect of Aromatics on the Thermal-Oxidative Stability of Synthetic Paraffinic Kerosene*, Energy & Fuels, 2014, 28, 3696–3703.
- [18] Boss B. D., Hazlett R. N., *Oxidation of hydrocarbons in the liquid phase: n-dodecane in a borosilicate glass chamber at 200°C*, Canadian Journal of Chemistry, 1969, 47, 4175-4182.
- [19] Rawson P.M., Stansfield C-A., Webster R.L., Evans D., Yildirim U., *The oxidative stability of synthetic fuels and fuel blends with monoaromatic blending components*, Fuel, 2015, 161, 97–104.
- [20] Zabarnick S., *Pseudo-Detailed Chemical Kinetic Modeling of Antioxidant Chemistry for Jet Fuel Applications*, Energy & Fuels, 1998, 12, 547-553.
- [21] Ervin J. S., Zabarnick S., *Computational Fluid Dynamics Simulations of Jet Fuel Oxidation Incorporating Pseudo-Detailed Chemical Kinetics*, Energy & Fuels, 1998, 12, 344-352.
- [22] Kuprowicz N. J., Ervin J.S. , Zabarnick S., *Modeling the liquid-phase oxidation of hydrocarbons over a range of temperatures and dissolved oxygen concentrations with pseudo-detailed chemical kinetics*, Fuel, 2004, 83 1795–1801.
- [23] Sander Z.H., West Z.J., Ervin J.S., Zabarnick S., *Experimental and Modeling Studies of Heat Transfer, Fluid Dynamics, and Autoxidation Chemistry in the Jet Fuel Thermal Oxidation Tester (JFTOT)*, Energy & Fuels 2015, 29, 7036–7047.
- [24] Zabarnick S., West Z.J., Shafer L.M. , Mueller S.S., Striebich R.C. *Studies of the Role of Heteroatomic Species in Jet Fuel Thermal Stability: Model Fuel Mixtures and Real Fuels*, Energy & Fuels, 2019, 33, 8557–8565.

- [25] Zhao L., Liu J., Zhang X., *Influencing Factors of Autoxidation Kinetics, Parameters of Endothermic Hydrocarbon Fuels*, Energy & Fuels, 2019, 33, 9, 8101–8109.
- [26] Clark R., K. M. Delargy K.M., Heins R.J., *The role of a metal deactivator in improving the thermal stability of aviation kerosines*, Proceedings of the 3rd International Conference on Stability and Handling of Liquid Fuels, 1988, 283–293.
- [27] Chin J.S., Lefebvre A.H., Sun F.T.Y., *Temperature effects on fuel thermal stability*, J. Eng. Gas Turbines Power, 1992, 114, 353–358.
- [28] Edwards T., Zabarnick S., *Supercritical Fuel Deposition Mechanisms*, Ind. Eng. Chem. Res., Vol. 32, No. 12, 1993, 3117-3122.
- [29] Marteney P.J., Spadaccini L.J., *Thermal decomposition of aircraft fuel*, J. Eng. Gas Turbines Power, 1986, 108, 648–653.
- [30] Altin O., Eser S., Orh F., Zhang, *Effects of thermal stressing conditions on carbon deposition from jet fuel decomposition*, 24th Biennial Conference on Carbon, 1999, 814–815.
- [31] Kendall D.R., Mills J.S., *The influence of JFTOT operating parameters on the assessment of fuel thermal stability*, SAE Technical Paper, 1985.
- [32] Clark R.H., Thomas L., *An investigation of the physical and chemical factors affecting the performance of fuels in the JFTOT*, SAE Technical Paper, 1988.
- [33] Jones E.G., W.J. Balster, J.M. Pickard, *Surface fouling in aviation fuels: an isothermal chemical study*, J. Eng. Gas Turbines Power, 1996, 118, 286–291.
- [34] Douthip, T., Ervin J.; Zabarnick S., Williams T. *Simulation of the effect of metal-surface catalysis on the thermal oxidation of jet fuel*, Energy & Fuels, 2004, 18, 2, 425–437.
- [35] Jones E. G., Balster W.J., *Phenomenological Study of the Formation of Insolubles in a Jet-A Fuel*, Energy & Fuels, 1993, 7, 968-977.
- [36] Balster W. J., Jones E.G., *Effects of temperature on formation of insoluble in aviation fuels*, The International Gas Turbine & Aeroengine Congress & Exhibition, 1997.
- [37] Winkler D.E., Hearne G.W., *Liquid Phase Oxidation of Isobutane*, Industrial and Engineering Chemistry, 1961, 53, 655-658.
- [38] Mayo F.R., *Free-radical Autoxidation of Hydrocarbons*, Accounts of Chemical Research, 1968, 1, 7,193-201.
- [39] Ingold K.U., *Peroxy Radicals*, Accounts of Chemical Research, 1969, 2, 1, 1-9.
- [40] Jensen R. K., Korcek S., Mahoney L. R., Zinbo M., *Elevated Temperatures. I. The Stirred Flow Reactor Technique and Analysis of Primary Products from n-Hexadecane Autoxidation at 120-180 °C*, Journal of the American Chemical Society, 1979 ,101,25 ,7574-7584.

- [41] Just G., Pritzkow W., Rudole M., Tien T.D., Voerckel V., *Estimation of Relative Autoxidation Rates of Normal Paraffins, Secondary Alcohols, and Ketones by Competitive Reactions*, Journal fur praktische Chemie, 1986, 328, 4, 469-660.
- [42] Garcia-Ochoa F., Romero A., Querol J., *Modeling of the Thermal n-Octane Oxidation in the Liquid Phase*, Ind. Eng. Chem. Res., 1989, 28, 43-48.
- [43] Rawson, P. M., Stansfield, C.-A., Creek, J., Webster, R. L., & Evans, D. J. *Suitability of a radical based method for assessment of jet fuel antioxidant capacity and projected storage stability*, Fuel, 2017, 199, 497–503.
- [44] Simic M.G., *Free Radical Mechanisms in Autoxidation Processes*, Journal of Chemical Education, 1981, 58, 2, 125-131.
- [45] Siouris S., Blakey S., *Fitness functions for evolutionary optimization of rate parameters in chemically reacting systems*, Chemical Engineering Science, 2019, 196, 16, 354-365.
- [46] Zabarnick S., *Chemical Kinetic Modeling of Jet Fuel Autoxidation and Antioxidant Chemistry*, Ind. Eng. Chem. Res., 1993, 32, 1012-1017.
- [47] Heneghan S. P., Zabarnick S., *Oxidation of jet fuels and the formation of Deposits*, Fuel, 1994, 73, p.1.
- [48] Dagaut P., Cathonnet M., Boetiner J.C., Gaillard F., *Kinetic Modeling of Propane Oxidation*, Combustion Science and Technology, 1987, 56, 23-03
- [49] West, Dissertation, *Studies of Jet fuel autoxidation chemistry: Catalytic hydroperoxydes decomposition & High heat flux effects*, The School of Engineering of the University of Dayton, 2011.
- [50] Spadaccini L. J., Huang H., *On-Line Fuel Deoxygenation for Coke Suppression*, Journal of Engineering for Gas Turbines and Power, 2003, 125, 686-692.
- [51] Kuprowicz, N. J., Zabarnick, S. West, Z. J., Ervin J. S. *Use of Measured Species Class Concentrations with Chemical Kinetic Modeling for the Prediction of Autoxidation and Deposition of Jet Fuels*, Energy & Fuels, 2007, 21, 530-544.
- [52] Pfaendtner J., Broadbelt L. J., *Mechanistic Modeling of Lubricant Degradation. 2. The Autoxidation of Decane and Octane*, Ind. Eng. Chem. Res., 2008, 47, 2897-2904.
- [53] Boss B. D., Hazlett R. N., *n-Dodecane Oxidation-Elucidation by Internal Reference Techniques*, Ind. Eng. Chem., Prod. Res. Dev., 1975, 14, 2, 135-138.
- [54] Hazlett R. N., Hall J. M., Matson M., *Reactions of Aerated N-Dodecane Liquid Flowing over Heated Metal Tubes*, Ind. Eng. Chem., Prod. Res. Dev., 1977 16, 2, 171-177.
- [55] Sheikhsari A., Alborzi E., Christopher Parks C, Siouris S. Blakey S., *Investigation of Aviation Lubricant Aging under Engine Representative Conditions*, Tribology Transactions, 2020, DOI: 10.1080/10402004.2020.1862378.

- [56] Heneghan S. P., Zabarnick S., Ballal D. R., Harrison, III W. E., *JP-8+100 - The development of high thermal stability jet fuel*, AIAA 34th Aerospace Sciences Meeting and Exhibit, Reno, NV Jan 15-18, 1996.
- [57] Grinstead B., Zabarnick, S., *Studies of Jet Fuel Thermal Stability, Oxidation, and Additives Using an Isothermal Oxidation Apparatus Equipped with an Oxygen Sensor*, Energy & Fuels, 1999, 13, 756-760.
- [58] Heneghan S.P., Schulz W., *Static Test of Jet Fuel Thermal and Oxidative Stability*, Journal of Propulsion and Power, 1993, 9, 1, 5-9.
- [59] Reddy K. T., Cernansky N. P., *Modified Reaction Mechanism of Aerated n-Dodecane Liquid Flowing over Heated Metal Tubes*, Energy & Fuels, 1988, 2, 205-213.
- [60] Martin, S. J., Granstaff, V. E., Frye, G. C., *Characterization of a Quartz Crystal Microbalance With Simultaneous Mass and Liquid Loading*, Analytical Chemistry, 1991, 63, 2272-2281.
- [61] Zabarnick S., Grinstead R.R., *Studies of Jet Fuel Additives Using the Quartz Crystal Microbalance and Pressure Monitoring at 140 °C*, Ind. Eng. Chem. Res., 1994, 33, 2771-2777.
- [62] Zabarnick S., *Studies of Jet Fuel Thermal Stability and Oxidation Using a Quartz Crystal Microbalance and Pressure Measurements*, Ind. Eng. Chem. Res., 1994, 33, 1348-1354.
- [63] Zabarnick S., Zelesnik P., Grinstead R. R., *Jet Fuel Deposition and Oxidation: Dilution, Materials, Oxygen, and Temperature Effects*, Journal of Engineering for Gas Turbines and Power, 1996, 118, 271-277.
- [64] Zabarnick S., Whitacre S.D., *Aspects of Jet Fuel Oxidation*, Journal of Engineering for Gas Turbines and Power, 1998, 120, 519-52.
- [65] Corporan E., Edwards T., Shafer L., DeWitt M.J., Klingshirn C., Zabarnick S., West Z., Striebich R., Graham J., Klein J., *Chemical, Thermal Stability, Seal Swell, and Emissions Studies of Alternative Jet Fuels*, Energy & Fuels, 2011, 25, 955-966.
- [66] Heneghan S. P., Zabarnick S., Ballal D. R., Harrison, III W. E., *JP-8+100 - The development of high thermal stability jet fuel*, AIAA 34th Aerospace Sciences Meeting and Exhibit, Reno, NV Jan 15-18, 1996.
- [67] Blin-Simiand N., Jorand F., Sahetchian K., *Hydroperoxides With Zero, One, Two or More Carbonyl Groups Formed During the Oxidation of N-Dodecane*, Combustion and Flame, 2001, 126, 1524-1532.
- [68] Pullen J., Saeed K., *An overview of biodiesel oxidation stability*, Renewable and Sustainable Energy Reviews, 2012, 16, 5924-5950.
- [69] Machado Y.L, Teles U.M., Neto A.A. D., Dantas T.N.C., Fonseca J.L.C., *Determination of antioxidant depletion kinetics using ASTM D 7545 as the accelerated oxidation method*, Fuel, 2013, 112, 172-177.
- [70] Araújo S.V., Luna F.M.T., Rola E.M, Azevedo D.C.S., Cavalcante C. L., *A rapid method for evaluation of the oxidation stability of castor oil FAME: influence of antioxidant type and concentration*, Fuel Processing Technology, 2009, 90, 1272-1277.

- [71] Ben Amara A., Nicolle A., Alves-Fortunato M., Jeuland Nicolas, *Toward Predictive Modeling of Petroleum and Biobased Fuel Stability: Kinetics of Methyl Oleate/n-Dodecane Autoxidation*, *Energy & Fuels*, 2013, 27, 6125–6133.
- [72] Rawson P.M., Webster R.L., Evans D., Abanteriba S., *Contribution of sulfur compounds to deposit formation in jet fuels at 140 °C using a quartz crystal microbalance technique*, *Fuel*, 2018, 231, 1, 1-7.
- [73] Alves-Fortunato M., Ayoub E., Bacha K., Dalmazzone C., *Fatty Acids Methyl Esters (FAME) autoxidation: New insights on insoluble deposit formation process in biofuels*, *Fuel*, 2020, 268, 1170-1174.
- [74] Dubrulle L., Lebeuf R., Fressancourt-Collinet M., Nardello-Rataj V., *Optimization of the vegetable oil composition in alkyd resins: A kinetic approach based on FAMEs autoxidation*, *Progress in Organic Coatings*, 2017, 112, 288–294.
- [75] Araújo S.V., Rocha B.S., Luna F.M.T., Rola E.M. Azevedo D.C.S., Cavalcante C. L. *FTIR assessment of the oxidation process of castor oil FAME submitted to PetroOXY and Rancimat methods*, *Fuel Processing Technology*, 2011, 92, 1152–1155.
- [76] Botella L., Bimbela F., Martín L., Arauzo J., Sánchez J.L., *Oxidation stability of biodiesel fuels and blends using the Rancimat and PetroOXY methods. Effect of 4-allyl-2,6-dimethoxyphenol and catechol as biodiesel additives on oxidation stability*, *Frontiers in Chemistry, Chemical Engineering*, 2014, 43, 2.
- [77] Bacha K., Ben-Amara A., Vannier A., Alves-Fortunato M., Nardin M., *Oxidation Stability of Diesel/Biodiesel Fuels Measured by a PetroOxy Device and Characterization of Oxidation Products*, *Energy Fuels*, 2015, 29, 4345–4355.
- [78] Kerkering S., Koch W., Andersson J. T., *Influence of Phenols on the Oxidation Stability of Home Heating Oil's/FAME Blends*, *Energy & Fuels*, 2015, 29, 793–799.
- [79] Marteau C., Ruyffelaere F., Aubry J.-M., Penverne C., Favier D., Nardello-Rataj V., *Oxidative degradation of fragrant aldehydes, Autoxidation by molecular oxygen*, *Tetrahedron*, 2013, 69, 2268-2275.
- [80] Moity L., Benazzouz A., Molinier V., Nardello-Rataj V., Elmkaddem M.K., De Caro P., Thiébaud-Roux S., Gerbaud V., Marion P., Aubry J.M., *Glycerol acetals and ketals as bio-based solvents: positioning in Hansen and COSMO-RS spaces, volatility and stability towards hydrolysis and autoxidation*, *Green Chem.*, 2015, 17, 1779-1792.
- [81] Sicard M., Boulicault J., Coulon K., Thomasset C., Ancelle J., Raepsaet, B. and Ser, F. *Oxidation stability of jet fuel model molecules evaluated by rapid small scale oxidation tests*, *The 13th International Conference on Stability, Handling and Use of Liquid Fuels, IASH 2013*.
- [82] Chatelain K., Nicolle A., Ben Amara A., Catoire L., Starck L., *Wide Range Experimental and Kinetic Modeling Study of Chain Length Impact on n-Alkanes Autoxidation*, *Energy & Fuels*, 2016, 30, 1294–1303.

- [83] Chatelain K., Nicolle A., Ben Amara A., Starck L., Catoire L., *Structure–Reactivity Relationships in Fuel Stability: Experimental and Kinetic Modeling Study of Isoparaffin Autoxidation*, *Energy & Fuels* 2018, 32, 9415–9426.
- [84] ASTM D7545 - 09 *Standard Test Method for Oxidation Stability of Middle Distillate Fuels—Rapid Small Scale Oxidation Test (RSSOT)*, ASTM International: West Conshohocken, PA, 2009.
- [85] Moffat R.J., *Describing the uncertainties in experimental results*, *Experimental Thermal and Fluid Science*, 1988, 1, 1, 3-17.
- [86] West Z.J., Zabarnick S., Striebich R.C., *Determination of Hydroperoxides in Jet Fuel via Reaction with Triphenylphosphine*, *Ind. Eng. Chem. Res.*, 2005, 44, 3377-3383.
- [87] Wiklund P., Karlsson C., Levin M., *Determination of Hydroperoxide Content in Complex Hydrocarbon Mixtures by Gas Chromatography/Mass Spectrometry*, *Analytical Sciences*, 2009, 25, 431-436.
- [88] ASTM D 3703-13 - *Standard Test Method for Hydroperoxide Number of Aviation Turbine Fuels, Gasoline and Diesel Fuels*, ASTM International: West Conshohocken, PA, 2013.
- [89] Zongo M.W., *Etude de l'oxydation des huiles de poisson micro encapsulées par DSC sous pression*, 2009.
- [90] ASTM D1655-18B - *Standard Specification for Aviation Turbine Fuels.*, ASTM International: West Conshohocken, PA, 20118.
- [91] ASTM D3242-08 - *Standard Test Method for Acidity in Aviation Turbine Fuel.*, ASTM International: West Conshohocken, PA, 2008.
- [92] Sarathy S.M., Westbrook C.K, Mehl M., Pitz W.J., Togbe C., Dagaut P., Wang H., Oehlschlaeger M.A., Niemann U., Seshadri K., Veloo P.S., Ji C., Egolfopoulos F.N., Lu T., *Comprehensive chemical kinetic modeling of the oxidation of 2-methylalkanes from C7 to C20*, *Combustion and Flame*, 2011, 158, 2338–2357.
- [93] Dagaut P., Reuillon M., Cathonnet M., *High Pressure Oxidation of Liquid Fuels From Low to High Temperature. 1. n-Heptane and iso-Octane*, *Combustion Science and Technology*, 1994, 95, 233-260.
- [94] Osmont A., Catoire L., Gokalp I., Swihart M.T., *Thermochemistry of C-C and C-H Bond Breaking in Fatty Acid Methyl Esters*, *Energy & Fuels* 2007, 21, 2027-2032.
- [95] Bugler J., Rodriguez A., Herbinet O., Battin-Leclerc F., Togbé C., Dayma G., Dagaut D., Curran H.J., *An experimental and modelling study of n-pentane oxidation in two jet-stirred reactors: The importance of pressure-dependent kinetics and new reaction pathways*, *Proceedings of the Combustion Institute*, 2016, 1–8.
- [96] Wang Z., Mohamed S.Y., Zhang L., Moshhammer K., Popolan-Vaida D.M., Shankar V.S.B., Lucassen A., Ruwe L., Hansen N., Dagaut P., Sarathy S.M., *New insights into the low-temperature oxidation of 2-methylhexane*, *Proceedings of the Combustion Institute*, 2017, 36, 373–382.

- [97] Wang Z., Chen B., Moshhammer K., Popolan-Vaida D.M., Sioud S., Shankar V.S.B., Vuilleumier D., Tao T., Ruwe L., Bräuer E., Hansen N., Dagaut P., Kohse-Höinghaus K., Raji M.A., Sarathy M., *n - Heptane cool flame chemistry: Unraveling intermediate species measured in a stirred reactor and motored engine*, Combustion and Flame, 2018, 187, 199–216.
- [98] Jalan A., Alecu I.M., Meana-Pañeda R., Aguilera-Iparraguirre J., Yang K.R., Merchant S.S., Truhlar D.G., Green W.H., *New Pathways for Formation of Acids and Carbonyl Products in Low- Temperature Oxidation: The Korcek Decomposition of γ -Ketohydroperoxides*, J. Am. Chem. Soc., 2013, 135, 11100–11114.
- [99] Thomas, J.R. *The Thermal Decomposition of Alkyl Hydroperoxides*. J. Am. Chem. Soc., 1955, 77, 246-248.
- [100] Emanuel', N.M., *The Oxidation of Hydrocarbons in the Liquid Phase*, Elsevier, 2013 - 424 pages.

AUTHOR INFORMATION

Corresponding Author

*Dr. Mickaël SICARD, e-mail mickael.sicard@onera.fr

Author Contributions

The manuscript was written through contributions of all authors. All authors have given approval to the final version of the manuscript. These authors contributed equally. (match statement to author names with a symbol)

ABBREVIATIONS

ATR	Attenuated Total Reflectance
FID	Flame Ionization Detector
FTIR	Fourier Transform Infrared Spectroscopy
GC/MS	Gas Chromatograph coupled to a Mass Spectrometer
PV	Peroxide Value
RSSOT	Rapid Small Scale Oxidation Test
TAN	Total Acid Number
TCD	Thermal Conductivity Detectors
TPP	TriPhenylPhosphine

